Research Square

Preprints are preliminary reports that have not undergone peer review.
They should not be considered conclusive, used to inform clinical practice,
or referenced by the media as validated information.

Whole-Electrolyte Design Enables Concentrated Two-Electron Storage of Viologens

Ryoichi Kanega

r-kanega@aist.go.jp

National Institute of Advanced Industrial Science and Technology https://orcid.org/0000-0003-0790-956X

Keito Sawahara

National Institute of Advanced Industrial Science and Technology

Miyuki Uchiyama

National Institute of Advanced Industrial Science and Technology

Mariko Saitou

National Institute of Advanced Industrial Science and Technology

Erika Ishida

National Institute of Advanced Industrial Science and Technology

Chieko Suzuki

National Institute of Advanced Industrial Science and Technology

Eiji Hosono

National Institute of Advanced Industrial Science and Technology

Daisuke Asakura

National Institute of Advanced Industrial Science and Technology https://orcid.org/0000-0001-7502-8858

Yoongkee Choe

National Institute of Advanced Industrial Science and Technology (AIST) https://orcid.org/0000-0002-9061-3761

Yukari Sato

National Institute of Advanced Industrial Science and Technology

Takashi Funaki

National Institute of Advanced Industrial Science and Technology

Akihiro Ohira

National Institute of Advanced Industrial Science and Technology https://orcid.org/0000-0002-5748-4830

Article

Keywords:

Posted Date: November 9th, 2026

DOI: https://doi.org/10.21203/rs.3.rs-11185436/v1

License: This work is licensed under a Creative Commons Attribution 4.0 International License.
Read Full License

Additional Declarations: There is **NO** Competing Interest.

Whole-Electrolyte Design Enables Concentrated Two-Electron Storage of Viologens

Ryoichi Kanega[1*], Keito Sawahara[1], Miyuki Uchiyama[1], Mariko Saitou[1], Erika Ishida[1], Chieko Suzuki[1], Eiji Hosono[1], Daisuke Asakura[1], Yoong-Kee Choe[2], Yukari Sato[1], Takashi Funaki[1] and Akihiro Ohira[1*]

[1]Research Institute for Energy Efficient Technologies, National Institute of Advanced Industrial Science and Technology, Tsukuba Central 5, 1-1-1 Higashi, Tsukuba, Ibaraki, 305-8565, Japan
[2]Materials DX Research Center, National Institute of Advanced Industrial Science and Technology, Tsukuba Central 2, 1-1-1 Umezono, Tsukuba, Ibaraki, 305-8568, Japan
*Correspondence: r-kanega@aist.go.jp, a-oohira@aist.go.jp

Abstract

Accessing the second reduction of viologens can double their charge-storage capacity, but at high concentrations the doubly reduced species associate into poorly soluble assemblies. Efforts to address this have focused on covalent modification of the redox-active molecule. Here we show that the surrounding electrolyte can instead be designed to regulate this association. Charge-matched aromatic ions, $PhSO_3^-$ and $PhN(Me)_3^+$, suppress capacity loss while leaving viologen redox potentials largely unchanged. Structural screening reveals that this function requires charge compatibility with the viologen, an aromatic framework and an appropriate counter anion. DFT calculations and diffusion measurements indicate that $PhN(Me)_3^+$ can interpose between reduced viologens and weaken their direct association, whereas NaCl stabilizes compact assemblies. Using this approach, an existing viologen supports reversible two-electron storage at 1.0 M, delivering a maximum capacity of 39.3 Ah L^{-1} over 100 cycles. These results establish the electrolyte as an active design parameter for controlling molecular association in concentrated multielectron redox chemistry.

Introduction

Viologens are among the most widely studied redox-active molecules for neutral aqueous organic redox flow batteries because of their high water solubility, structural tunability and reversible redox chemistry.[1-5] Although conventional viologens are commonly operated through a one-electron redox process, accessing the second reduction can in principle double their molecular charge storage capacity. Recent studies have sought to realize reversible two-electron viologen chemistry through molecular engineering of the active material.[6-10] These designs combine modifications of the π-conjugated framework and peripheral substituents to tune the redox energetics while maintaining sufficient solubility and stability of the reduced states. For example, π-conjugation extension can decrease the potential separation between the two sequential reductions, whereas charged and solvation-promoting substituents can help retain aqueous compatibility upon deep reduction.[11-13]

Despite these advances in molecular design, translating two-electron viologen chemistry to highly concentrated electrolytes remains challenging. As the redox-active bipyridinium framework is deeply reduced, its positive charge density decreases, altering hydration and intermolecular interactions. At high active-material concentrations, these changes can promote association, aggregation and precipitation, thereby limiting the accessible two-electron capacity.[14,15] Reported approaches have largely addressed these problems by further modifying the redox-active molecule itself, for example through charged, sterically demanding or solvation-promoting substituents. Nevertheless, reversible two-electron flow-cell operation has so far been demonstrated mainly at viologen concentrations of 0.5 M or below (Supplementary Table 1). A conceptually distinct approach has instead treated association as a functional asset: π-dimerization of singly reduced pyridinium radicals lowers the free-radical fraction and thereby suppresses reactivity with dissolved oxygen.[16] Association is therefore not intrinsically detrimental, but is a control variable with an optimum. Beyond the radical dimer, the doubly reduced species, which is closed-shell and far less charged, can proceed to higher-order, poorly soluble assemblies, so that the limiting process becomes loss of soluble active material rather than radical–oxygen reactivity. Here we address this second regime, and ask which molecular elements of the surrounding electrolyte determine where the association equilibrium is arrested.

This molecular-centric approach implicitly treats the supporting electrolyte as a passive medium that provides ionic conductivity and charge balance. Yet the speciation, solvation and intermolecular interactions of charged redox molecules are inherently determined by their surrounding ionic environment.[17-21] We therefore asked whether two-electron viologen chemistry could instead be controlled by engineering the electrolyte around an existing redox-active molecule, without further modification of the viologen framework (Fig. 1a). Such an approach would shift the design principle

from optimization of an isolated redox molecule to control of the collective interactions within the electrolyte.

Here in this paper, we develop an electrolyte-level strategy that regulates the intermolecular environment of reduced viologens using aromatic ionic components, $PhSO_3Na$ and $PhN(Me)_3Cl$ (Fig. 1b). By systematically varying the charge and molecular structure of the supporting electrolyte components and comparing them with NaCl, we show that the stabilization cannot be explained by ionic strength or electrostatic repulsion alone (Fig. 1c). Experiments and theoretical calculations instead indicate that the aromatic $PhN(Me)_3^+$ component forms a preferential ion-mediated association with reduced viologen species, weakening the direct interaction between viologen units and suppressing their concentration-induced association. Importantly, this strategy does not substantially perturb the intrinsic redox potentials of the viologen.

This electrolyte engineering enables reversible two-electron storage at a viologen concentration of 1.0 M, delivering a maximum discharge capacity of 39.3 Ah L^{-1} during 100 cycle operation, corresponding to 73.3% utilization of the theoretical two-electron capacity, with an average capacity fade rate of 0.19% $cycle^{-1}$. These results demonstrate that the accessible redox chemistry of concentrated organic electrolytes is governed not only by the molecular structure of the active material but also by the interaction network created by the surrounding electrolyte components. More broadly, our findings establish whole-electrolyte interaction design as a route to controlling concentrated multi-electron redox chemistry.

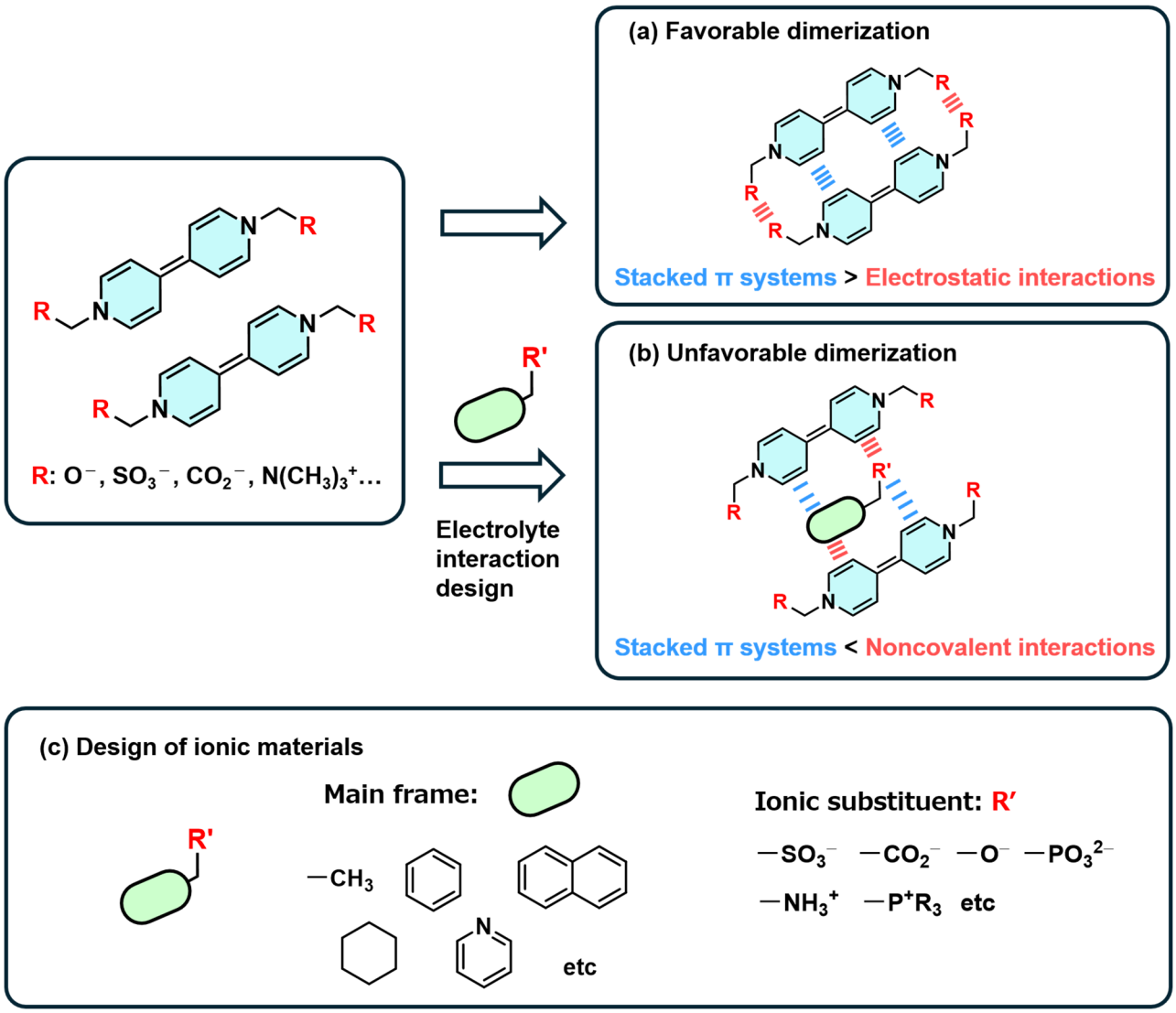


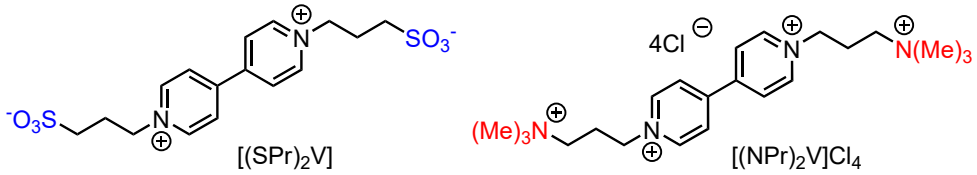
Fig. 1 | Molecular and electrolyte design strategies for concentrated two-electron viologen storage. **a,** Conventional molecular-design approaches introduce ionic or solvation-promoting substituents directly into the viologen framework to stabilize the two-electron reduced species. **b,** Electrolyte-level strategy developed in this work, in which charge matched aromatic electrolyte components regulate the association of reduced viologens without further covalent modification of the active material. **c,** Molecular parameters examined to identify the structural requirements for effective electrolyte regulation, including charge matching, counter anion, ammonium structure, aromatic framework and para substituent.

Results and discussion

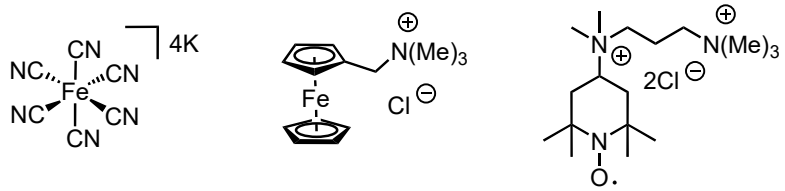
Electrolyte composition decouples redox thermodynamics from cycling stability

To examine whether the electrolyte composition can control the state of viologens after two-electron reduction, we combined the $[(SPr)_2V]$ and the $[(NPr)_2V]Cl_4$ with electrolytes containing NaCl, $PhSO_3Na$ or $PhN(Me)_3Cl$ (Fig. 2). We first asked whether the performance differences between these electrolytes originate from changes in the redox potentials themselves. For $[(SPr)_2V]$, a small difference was observed in the first redox process between the NaCl and $PhSO_3Na$ systems, whereas the second redox process showed no appreciable change (Fig. 3a). Similarly, the redox potentials of $[(NPr)_2V]Cl_4$ were almost the same in the NaCl and $PhN(Me)_3Cl$ systems (Fig. 3b). The electrolyte composition therefore does not substantially change the electron-transfer thermodynamics of the viologen, but rather acts on the intermolecular environment formed after reduction. In contrast to this thermodynamic similarity, the charge–discharge behavior depended strongly on the electrolyte composition (Fig. 3c). For the $[(SPr)_2V]/K_4[Fe(CN)_6]$ cell, the discharge capacity decreased sharply after about 10 cycles in the NaCl-containing electrolyte and stable operation became difficult within 20 cycles, whereas the capacity loss was clearly suppressed in the electrolyte containing $PhSO_3Na$ (Fig. 3d). The same trend was observed for the $[(NPr)_2V]Cl_4$/FcNCl cell: the discharge capacity decreased markedly in the NaCl system, while the stability was improved in the $PhN(Me)_3Cl$ system (Fig. 3e). The electrolyte composition is thus reflected much more strongly in the cycling stability than in the redox potentials, suggesting that it is involved in controlling the state of the reduced species.

(a) Negative active material



(b) Positive active material



(c) Negative electrolyte

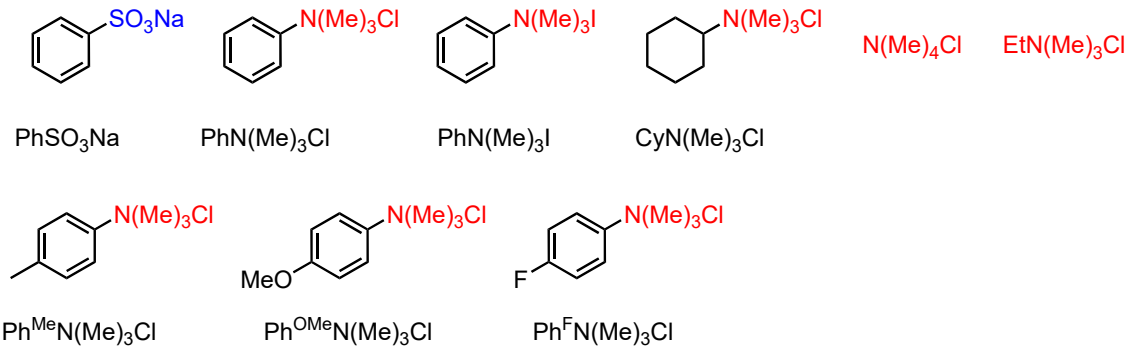


Fig. 2 | Redox-active materials and electrolyte components used in this work. a, Molecular structures of the negative active materials, the $[(SPr)_2V]$ and the $[(NPr)_2V]Cl_4$. **b,** Positive active materials used for full-cell evaluation: $K_4[Fe(CN)_6]$, FcNCl and $[N2\text{-}TEMPO]Cl_2$. **c,** Electrolyte components compared in this work.

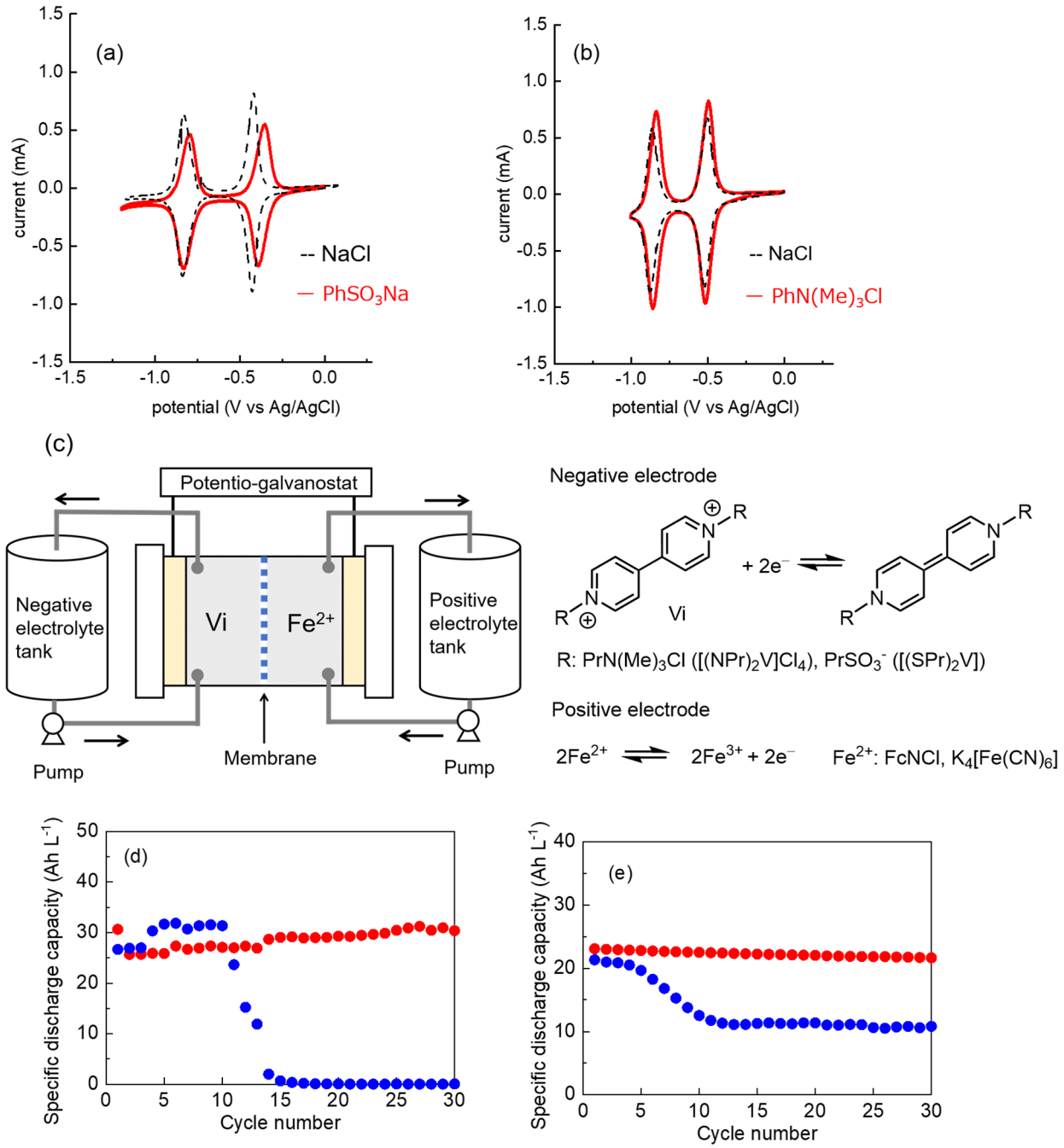


Fig. 3 | Effects of electrolyte composition on the electrochemical properties and full-cell cycling of viologen derivatives. a, Cyclic voltammograms of 10 mM $[(SPr)_2V]$ in electrolytes containing 0.1 M NaCl (black) or 0.1 M $PhSO_3Na$ (red). **b,** Cyclic voltammograms of 10 mM $[(NPr)_2V]Cl_4$ in electrolytes containing 0.1 M NaCl (black) or 0.1 M $PhN(Me)_3Cl$ (red). **c**, Schematic of the structural drawings showing the cell reactions of the viologen negative electrolyte and the Fe^{2+} positive electrolyte. **d,** Cycling performance of the 1.0 M $[(SPr)_2V]$/0.5 M $K_4[Fe(CN)_6]$ full cell using negative electrolytes containing 1.25 M NaCl (blue) or 1.25 M $PhSO_3Na$ (red) at 10 mA cm^{-2}. **e,** Cycling performance of the 0.5 M $[(NPr)_2V]Cl_4$/0.5 M FcNCl full cell using negative electrolytes containing 0.84 M NaCl (blue) or 0.84 M $PhN(Me)_3Cl$ (red) at 80 mA cm^{-2}.

Charge matching governs productive electrolyte–viologen association

To determine whether the effect of the aromatic electrolyte components simply arises from the presence of an aromatic ring, or whether it requires a specific charge relationship with the active material, we evaluated combinations in which the charge signs were deliberately mismatched. In the charge mismatched systems $[(NPr)_2V]Cl_4$/$PhSO_3Na$ and $[(SPr)_2V]$/$PhN(Me)_3Cl$, the cell voltage reached the upper cut-off limit immediately after the start of charging, and sustained charge–discharge operation could not be obtained (Supplementary Table 2 and Supplementary Fig. 9). This failure cannot be explained by a simple mismatch of ion transport across the membrane. Indeed, when the anion exchange membrane was replaced by a cation exchange membrane in the $[(NPr)_2V]Cl_4$/$PhSO_3Na$ system, the real part of the impedance decreased only partially, from 53.7 to 40.2 Ω cm^2; this value remained far above that of the charge matched systems, and the charge–discharge capability was not recovered. In all charge mismatched systems, the real resistance was markedly larger than in the charge matched systems (approximately 9–20 Ω cm^2 at 1 Hz), reaching about 270 Ω cm^2 at 1 Hz for the most strongly mismatched $[(SPr)_2V]$/$PhN(Me)_3Cl$ system. Because these measurements were carried out before the first charge, precipitation or pore blocking caused by cycling is unlikely to be the main origin of this difference. These results indicate that the effect of the aromatic electrolyte components is not obtained from the aromatic ring alone, but requires charge compatibility with the active material.[22]

Molecular structure defines the function of aromatic electrolyte components

If charge matching alone determined the function, ammonium components with the same charge sign would be expected to show a similar effect. We therefore used the relatively stable $[(NPr)_2V]Cl_4$ system and varied the counter anion, the ammonium structure, the aromatic framework and the para substituent in a stepwise manner, in order to separate the molecular elements required for the function (Table 1). Changing the counter anion of $PhN(Me)_3^+$ from Cl^- to I^- increased the cell resistance, and stable charge–discharge operation was not obtained (Table 1, Entry 2). This difference shows that the function involves not only the aromatic ammonium cation but also the local ionic environment, including the counter anion. The requirement for an aromatic framework was examined by comparison with $N(Me)_4Cl$, $EtN(Me)_3Cl$ and $CyN(Me)_3Cl$ (Table 1, Entries 3-5). None of them suppressed the capacity fade as effectively as $PhN(Me)_3Cl$, indicating that a positively charged ammonium moiety alone is not sufficient and that interactions involving the aromatic ring direct the association state of the reduced viologen. When the para substituent was varied, all of the substituted components showed a larger capacity fade than the unsubstituted $PhN(Me)_3Cl$ (Table 1, Entries 6-8). Although the capacity retention differed clearly between the electrolyte components, the coulombic efficiency was maintained above 95% in all systems except Entry 2 (Supplementary Fig. 10 and Supplementary Fig. 11). This result suggests that the observed performance differences cannot be explained by crossover or by charge loss through pronounced side reactions alone. The structural screening therefore shows that the function requires, in addition to charge matching, a specific structural combination of an unsubstituted phenyl group and a trimethylammonium moiety, and that it cannot be reduced to a single factor such as the presence of a positive charge or the introduction of an aromatic ring. In other words, the aromatic electrolyte component is not a passive supporting electrolyte but defines the intermolecular environment of the reduced viologen through short-range interactions that are sensitive to both electrostatic interactions and substituent structure. To clarify at the molecular level which differences in association mode correspond to this structural dependence, we next compared the association structures selected by NaCl and $PhN(Me)_3Cl$ using DFT calculations.

Table 1 | Effects of electrolyte component structure on the cycling performance of $[(NPr)_2V]Cl_4$/FcNCl system[a].

Entry	Electrolyte	Structural modification	Capacity fade rate (% cycle^{-1})	Coulombic efficiency (%)[b]
1	$PhN(Me)_3Cl$	Reference	0.15	99.3
2	$PhN(Me)_3I$	Counter anion $Cl^- \rightarrow I^-$	Limited[c]	Limited[c]
3	$CyN(Me)_3Cl$	Phenyl group → cyclohexyl	0.33	99.5
4	$N(Me)_4Cl$	Phenyl group → methyl	0.34	99.3
5	$EtN(Me)_3Cl$	Phenyl group → ethyl	0.92	96.9
6	$Ph^{Me}N(Me)_3Cl$	Para hydrogen → methyl	0.74	98.8
7	$Ph^{OMe}N(Me)_3Cl$	Para hydrogen → methoxy	0.85	98.5
8	$Ph^{F}N(Me)_3Cl$	Para hydrogen → fluorine	0.91	97.9

[a]0.5 M $[(NPr)_2V]Cl_4$ (8 mL)/0.5 M FcNCl (16 mL) containing 0.84 M electrolyte with FAA-3-PK-75. [b]Average over 100 cycles. [c]Charge–discharge could not be evaluated under the applied current density, as the high initial cell resistance caused the voltage to reach the cut-off limits.

Electrolyte dependent regulation of reduced viologen association

To interpret the relationships obtained from the structural screening at the molecular level, we compared, by DFT calculations, the additive-free dimer of the two-electron reduced species $[(NPr)_2V]Cl_2$ with association models containing NaCl or $PhN(Me)_3Cl$ (Fig. 4). The additive-free dimer adopted an L-shaped geometry, with a centroid-to-centroid distance between the viologen units of 4.62 Å and a dimerization energy of $\Delta E = -28.6$ kcal mol^{-1} (Fig. 4a). In the model containing NaCl, the centroid distance decreased to 3.85 Å and the formation energy became $\Delta E = -57.6$ kcal mol^{-1} (Fig. 4b). In the optimized structure, two Cl^- ions were located close to Na^+, suggesting that local ionic coordination can stabilize a compact association. In contrast, the model containing $PhN(Me)_3Cl$ gave a wedge-type structure in which $PhN(Me)_3^+$ is interposed between the two viologen units, increasing the centroid distance to 5.75 Å (Fig. 4c). Since the formation of this structure was also energetically favorable ($\Delta E = -28.6$ kcal mol^{-1}), $PhN(Me)_3^+$ is considered to interpose transiently between viologen units[23] and thereby weaken the direct interaction between them. We note, however, that this calculated structure is not intended to represent a major species that diffuses as an intact three-component assembly in solution; rather, it should be regarded as a molecular model of the local interaction mode by which the aromatic electrolyte component weakens direct viologen–viologen association. This interpretation is consistent with the diffusion behavior obtained from PGSE-NMR. The self-diffusion coefficient was 3.06×10^{-10} m^2 s^{-1} in the NaCl system, whereas it was about twice as large, 6.02×10^{-10} m^2 s^{-1}, in the $PhN(Me)_3Cl$ system (Supplementary Fig. 12 and Supplementary Table 3). Since the viscosities of the two electrolytes were nearly the same, this difference in diffusion coefficient is considered to reflect a difference in the effective size of the diffusing species rather than the solution viscosity (Supplementary Table 3).[24] That is, larger diffusing species become dominant in the presence of NaCl, whereas their formation is suppressed in the presence of $PhN(Me)_3Cl$ and the contribution of smaller species increases.[25] The aromatic electrolyte component therefore appears to suppress direct dimerization of the reduced viologen through local interposition, shifting the association equilibrium toward the free species. The dimerization promoted in the NaCl system may proceed further to higher-order assemblies and poorly soluble aggregates, leading to precipitation and decreasing the amount of active material that remains reversibly accessible in the electrolyte, and thus causing the capacity loss. In contrast, suppression of direct association by $PhN(Me)_3Cl$ mitigates the formation of poorly soluble assemblies and precipitates, maintaining the fraction of reduced viologen that remains reversibly accessible and thereby contributing to the improved cycling performance.

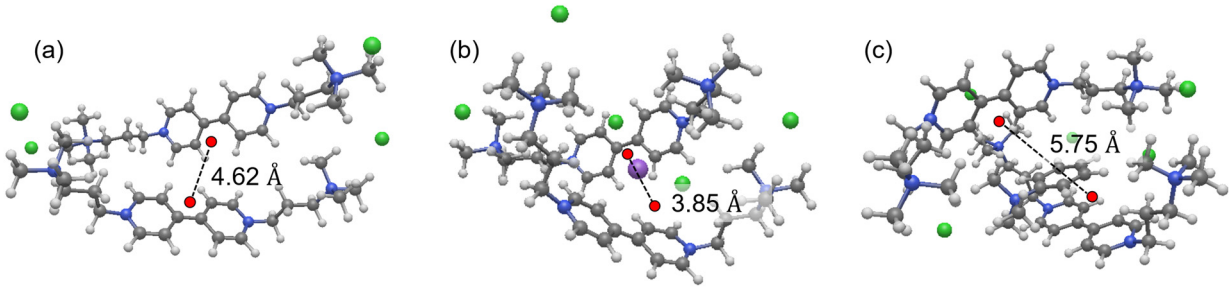


Fig. 4 | Electrolyte-dependent association structures of the two-electron reduced viologen obtained by DFT calculations. a, Optimized structure of the additive-free $[(NPr)_2V]Cl_2$ dimer, which adopts an L-shaped geometry with a viologen centroid-to-centroid distance of 4.62 Å ($\Delta E = -28.6$ kcal mol^{-1}). **b,** Optimized structure of the NaCl-containing assembly, which adopts a more compact geometry with a centroid-to-centroid distance of 3.85 Å ($\Delta E = -57.6$ kcal mol^{-1}). **c,** Optimized structure of the $PhN(Me)_3Cl$-containing assembly, which adopts an expanded wedge-type geometry in which $PhN(Me)_3^+$ is interposed between the two viologen units, increasing the centroid-to-centroid distance to 5.75 Å ($\Delta E = -28.6$ kcal mol^{-1}).

Translation of molecular assembly control to concentrated two-electron storage

To examine whether the electrolyte-directed selection of association structures also operates under concentrated conditions, where intermolecular interactions become more influential, we increased the concentration of the negative active material $[(NPr)_2V]Cl_4$ to 1.0 M and assembled a full cell using $[N2\text{-}TEMPO]Cl_2$ as the positive active material (Fig. 5a and Supplementary Fig. 13). The rate performance was evaluated at current densities of 40–120 mA cm^{-2}. Two voltage plateaus were observed in each charge–discharge curve, showing that the two-electron reaction proceeds through two sequential reduction steps even under concentrated conditions (Fig. 5b). At 40 mA cm^{-2}, a discharge capacity of 44.3 Ah L^{-1} was obtained, corresponding to a capacity utilization of 82.6%, suggesting that the control of association can mitigate the decrease in active-material utilization that accompanies an increase in concentration. In the subsequent cycling test at 60 mA cm^{-2}, the maximum discharge capacity based on the negative electrolyte volume reached 39.3 Ah L^{-1} (corresponding to 73.3% utilization of the active material), and the maximum energy density based on the total electrolyte volume reached 22.7 Wh L^{-1}. The cell operated over 100 cycles with a capacity fade rate of 0.19% $cycle^{-1}$ (Fig. 5c). The fact that a high two-electron capacity could be extracted at 1.0 M, where molecular association becomes pronounced, shows that the selection of association structures by aromatic electrolyte components is not a phenomenon limited to dilute conditions but can be developed into a design principle for concentrated electrolytes.

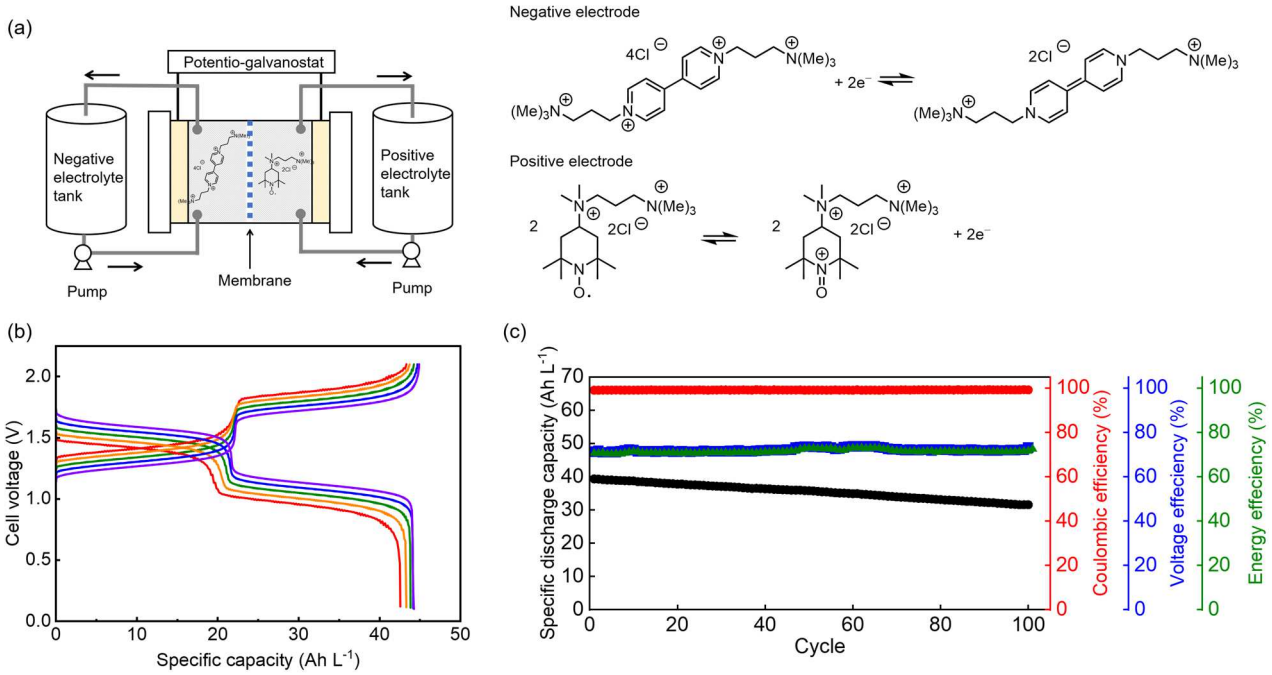


Fig. 5 | Concentrated two-electron storage enabled by electrolyte-directed viologen association. **a,** Schematic of the full cell employing 1.0 M $[(NPr)_2V]Cl_4$ as the negative active material and [N2-TEMPO]Cl_2 as the positive active material. **b,** Charge–discharge profiles recorded during the second cycle at current densities of 40–120 mA cm^{-2}, showing two voltage plateaus associated with the sequential two-electron redox processes of the viologen. **c,** Cycling performance of the full cell in a 100 cycle test at 60 mA cm^{-2}, showing the discharge capacity (left axis) and coulombic efficiency, voltage efficiency and energy efficiency (right axis).

Taken together, these results extend the role of the electrolyte from bulk ionic conduction to the selection of molecular association structures. The redox potentials were largely preserved while the cycling behavior changed substantially, the porous-electrode resistance became evident in the charge mismatched systems, and a dependence was found on both the molecular structure of the electrolyte component and the geometry of the resulting assembly. These observations indicate that the cell performance is determined not by the properties of the active material alone, but by an interaction network consisting of the active material, the electrolyte components, the solvent and the electrode interface. The design principle presented here is therefore not an empirical stabilization by a particular additive, but a whole-electrolyte interaction design in which charge matching and local non-covalent interactions are used to select a molecular assembly state that remains electrochemically accessible.

Conclusions

In conclusion, we demonstrated that two-electron storage in concentrated viologen electrolytes can be promoted by regulating non-covalent association through electrolyte composition rather than by further covalent modification of the active material. Electrolytes containing charge matched $PhSO_3Na$ or $PhN(Me)_3Cl$ improved cycling while largely preserving the intrinsic viologen redox potentials, whereas charge mismatched combinations generated pronounced porous-electrode resistance and prevented sustained operation. Structural screening showed that the function of $PhN(Me)_3Cl$ depends on the combined effects of charge compatibility, the aromatic framework, the counter anion and substituent-dependent hydrophobicity. DFT calculations provided a molecular interpretation of these trends: NaCl stabilized a compact reduced-viologen assembly, whereas $PhN(Me)_3Cl$ redirected association toward an expanded ion-mediated geometry in which the direct interaction between viologen units is weakened. Applying this design principle to a negative electrolyte containing 1.0 M $[(NPr)_2V]Cl_4$ enabled a maximum discharge capacity of 39.3 Ah L^{-1} and a maximum total-electrolyte-based energy density of 22.7 Wh L^{-1}, with operation over 100 cycles and an average capacity fade rate of 0.19% $cycle^{-1}$. Although further improvements in mass transport, electrode–electrolyte interfacial processes, membrane transport and electrolyte balance are required for longer-term operation, the present results show that selected electrolyte components can actively regulate molecular structure. This whole-electrolyte interaction design provides a general framework for controlling molecular assembly and accessing concentrated multi-electron redox chemistry in aqueous flow batteries.

Methods

General

^{1}H NMR and ^{13}C NMR spectra were recorded on a Bruker Avance 600 spectrometer. Electrochemical investigations were conducted using a Hokuto Denko HZ-Pro electrochemical measurement system. The chemicals and membranes were purchased from commercial suppliers and were used without further purification or treatment. [N2-TEMPO]Cl_2 was prepared according to previously reported methods.[23] [$(SPr)_2V$] and $EtN(Me)_3Cl$ were purchased from BLDpharm, Inc. [$(NPr)_2V$]Cl_4, $K_4[Fe(CN)_6]$, FcNCl, $PhSO_3Na$, $PhN(Me)_3Cl$, $PhN(Me)_3I$ and $N(Me)_4Cl$ were purchased from Tokyo Chemical Industry. $CyN(Me)_3Cl$, $Ph^{Me}N(Me)_3Cl$, $Ph^{OMe}N(Me)_3Cl$ and $Ph^{F}N(Me)_3Cl$ were synthesized as described in the Supplementary Information.

Electrochemical measurements

The cyclic voltammetry measurements used a three-electrode setup with the two-compartment experimental cell (Supplementary Fig. 14). The experimental cell was assembled with a carbon felt working (φ 5, AAF304ZS, Toyobo) and counter electrode (φ 10 mm), and Ag rod as reference electrode, E620K (Fumasep) or FAA-3-PK-75 (Fumasep). The potential difference between an Ag rod and an Ag/AgCl electrode was measured, and the potential was shown against the Ag/AgCl reference electrode (Supplementary Fig. 15). Cyclic voltammetry was conducted using 10 mM [$(SPr)_2V$] and 1.0 M NaCl in H_2O (counter: 0.1 M $K_4[Fe(CN)_6]$ and 1.0 M NaCl in H_2O) or 10 mM [$(NPr)_2V$]Cl_4 and 1.0 M NaCl in H_2O (counter: 0.1 M FcNCl and 1.0 M NaCl in H_2O). Cyclic voltammetry was also conducted using 10 mM [$(SPr)_2V$] and 1.0 M $PhSO_3Na$ in H_2O (counter: 0.1 M $K_4[Fe(CN)_6]$ and 1.0 M NaCl in H_2O) or 10 mM [$(NPr)_2V$]Cl_4 and 1.0 M $PhN(Me)_3Cl$ in H_2O (counter: 0.1 M FcNCl and 1.0 M NaCl in H_2O).

Electrochemical flow cell assembly and charge–discharge tests

Electrochemical flow cells were assembled in two configurations, and charge–discharge measurements were carried out in a simple glove bag purged with N_2. For the 0.5 M active-material tests, the cell consisted of an E620K or FAA-3-PK-75 membrane, carbon paper electrodes (2.23 cm × 2.23 cm × 0.37 mm, TGP-H-120, Toray), 0.2 mm-thick PTFE-based gaskets, and a frame equipped with graphite and gold current collectors (Supplementary Fig. 16a). The carbon paper electrodes were heat-treated in air at 800 °C for 2 h before use. Charge–discharge tests were conducted using 0.5 M [$(SPr)_2V$] and 0.84 M NaCl or $PhSO_3Na$ in H_2O (positive electrolyte: 0.5 M $K_4[Fe(CN)_6]$ in H_2O), or using 0.5 M [$(NPr)_2V$]Cl_4 and 0.84 M NaCl or $PhN(Me)_3Cl$ in H_2O (positive electrolyte: 0.5 M FcNCl

in H_2O). The negative and positive electrolyte volumes were 8 and 16 mL, respectively, and the electrolytes were circulated at 20 mL min^{-1}. Charge–discharge tests were performed between 1.9 and 0 V at 10 mA cm^{-2} for the $[(SPr)_2V]/K_4[Fe(CN)_6]$ cells and at 80 mA cm^{-2} for the $[(NPr)_2V]Cl_4$/FcNCl cells (Supplementary Fig. 17). For the 1.0 M active-material tests, the cell consisted of a DSVN membrane (AGC), carbon felt electrodes (2.5 cm × 1 cm × 3 mm, AAF304ZS, Toyobo), 3 mm-thick silicone rubber gaskets, and an ebonite frame equipped with graphite/gold current collectors (Supplementary Fig. 16b). The carbon felt electrodes were heat-treated in air at 500 °C for 1 h before use. Charge–discharge tests were conducted using 1.0 M $[(NPr)_2V]Cl_4$ and 1.67 M $PhN(Me)_3Cl$ in H_2O (positive electrolyte: 0.5 M [N2-TEMPO]Cl_2 in H_2O). Charge–discharge tests were performed between 2.1 and 0.1 V (Supplementary Fig. 17). Rate tests were conducted at 40–120 mA cm^{-2} using 5 mL of negative electrolyte and 20 mL of positive electrolyte, whereas the 100 cycle test was conducted at 60 mA cm^{-2} using 5 mL of negative electrolyte and 17 mL of positive electrolyte. In both 1.0 M-cell measurements, the electrolytes were circulated at 15 mL min^{-1}. A peristaltic pump with Tygon tubing was used for electrolyte circulation. The discharge capacity, coulombic efficiency, voltage efficiency, energy efficiency and capacity retention were calculated according to the following equations:

Discharge capacity: $I_{\mathrm{Discharge}}\ (\mathrm{mA}) \times t\ (\mathrm{h})$

Coulombic efficiency (%): $\frac{I_{\mathrm{Discharge}}\ (\mathrm{mA}) \times t\ (\mathrm{h})}{I_{\mathrm{Charge}}\ (\mathrm{mA}) \times t\ (\mathrm{h})} \times 100$

Voltage efficiency (%): $\frac{Average\ cell\ voltage_{\mathrm{Discharge}}\ (\mathrm{V})}{Average\ cell\ voltage_{\mathrm{Charge}}\ (\mathrm{V})} \times 100$

Energy efficiency (%): Coulombic efficiency×Voltage efficiency

Capacity retention (% $cycle^{-1}$): $\frac{[I_{\mathrm{Discharge}}\ (\mathrm{mA}) \times t\ (\mathrm{h})]_{\mathrm{n\ cycle}}}{[I_{\mathrm{Discharge}}\ (\mathrm{mA}) \times t\ (\mathrm{h})]_{\mathrm{1\ cycle}}} \times \frac{1}{\mathrm{n\ (cycle)}} \times 100$

Data availability

All data presented in this study are provided in the Supplementary Information.

Author contributions

R.K. and A.O. conceived the study and designed the experiments. R.K., K.S., M.U., M.S., E.I. and A.O. performed the electrochemical measurements. R.K., K.S., C.S., E.I. and T.F. carried out the synthesis. R.K. and Y.-K.C. performed the theoretical calculations. R.K., K.S., E.H., D.A., Y.-K.C.,

Y.S., T.F. and A.O. analyzed the data and co-wrote the manuscript. All authors discussed the results and commented on the manuscript.

Acknowledgments

We acknowledge Grants-in-Aid for Scientific Research (JPMJAN25A1, 25K01888 and JPNP14004) from Japan Science and Technology Agency, Japan Society for the Promotion of Science and New Energy and Industrial Technology Development Organization.

Competing interests

The authors declare no competing interests.

References

1 Janoschka, T. *et al.* An aqueous, polymer-based redox-flow battery using non-corrosive, safe, and low-cost materials. *Nature* **527**, 78–81 (2015). 10.1038/nature15746

2 Liu, T., Wei, X., Nie, Z., Sprenkle, V. & Wang, W. A Total Organic Aqueous Redox Flow Battery Employing a Low Cost and Sustainable Methyl Viologen Anolyte and 4-HO-TEMPO Catholyte. *Adv. Energy Mater.* **6**, 1501449 (2016). 10.1002/aenm.201501449

3 Beh, E. S. *et al.* A Neutral pH Aqueous Organic–Organometallic Redox Flow Battery with Extremely High Capacity Retention. *ACS Energy Letters* **2**, 639–644 (2017). 10.1021/acsenergylett.7b00019

4 Hu, B., DeBruler, C., Rhodes, Z. & Liu, T. L. Long-Cycling Aqueous Organic Redox Flow Battery (AORFB) toward Sustainable and Safe Energy Storage. *Journal of the American Chemical Society* **139**, 1207–1214 (2017). 10.1021/jacs.6b10984

5 DeBruler, C., Hu, B., Moss, J., Luo, J. & Liu, T. L. A Sulfonate-Functionalized Viologen Enabling Neutral Cation Exchange, Aqueous Organic Redox Flow Batteries toward Renewable Energy Storage. *ACS Energy Letters* **3**, 663–668 (2018). 10.1021/acsenergylett.7b01302

6 DeBruler, C. *et al.* Designer Two-Electron Storage Viologen Anolyte Materials for Neutral Aqueous Organic Redox Flow Batteries. *Chem* **3**, 961–978 (2017). 10.1016/j.chempr.2017.11.001

7 Pan, M. *et al.* The Dual Role of Bridging Phenylene in an Extended Bipyridine System for High-Voltage and Stable Two-Electron Storage in Redox Flow Batteries. *ACS Appl. Mater. Interfaces* **13**, 44174–44183 (2021). 10.1021/acsami.1c09019

8 Pan, M. *et al.* Reversible Redox Chemistry in Pyrrolidinium-Based TEMPO Radical and Extended Viologen for High-Voltage and Long-Life Aqueous Redox Flow Batteries. *Adv. Energy Mater.* **12**, 2103478 (2022). 10.1002/aenm.202103478

9 Liu, Y. *et al.* A Highly Soluble Two-Electron Storage Viologen Negolyte for Neutral Aqueous

Organic Redox Flow Batteries. *ACS Omega* **10**, 18641–18649 (2025). 10.1021/acsomega.4c11656

10 Yin, T., Duanmu, J. & Liu, L. Viologen-based aqueous organic redox flow batteries: materials synthesis, properties, and cell performance. *J. Mater. Chem. A* **12**, 15519–15540 (2024). 10.1039/D4TA00753K

11 Luo, J., Hu, B., Debruler, C. & Liu, T. L. A π-Conjugation Extended Viologen as a Two-Electron Storage Anolyte for Total Organic Aqueous Redox Flow Batteries. *Angew. Chem. Int. Ed.* **57**, 231–235 (2018). 10.1002/anie.201710517

12 Hu, S. *et al.* Phenylene-Bridged Bispyridinium with High Capacity and Stability for Aqueous Flow Batteries. *Adv. Mater.* **33**, 2005839 (2021). 10.1002/adma.202005839

13 Tang, G. *et al.* Designing Robust Two-Electron Storage Extended Bipyridinium Anolytes for pH-Neutral Aqueous Organic Redox Flow Batteries. *JACS Au* **2**, 1214–1222 (2022). 10.1021/jacsau.2c00184

14 Bird, C. L. & Kuhn, A. T. Electrochemistry of the viologens. *Chem. Soc. Rev.* **10**, 49–82 (1981). 10.1039/cs9811000049

15 Nikumbe, D. Y. *et al.* Stability of monoradical cation dimer of viologen derivatives in aqueous redox flow battery. *J. Appl. Electrochem.* **54**, 2165–2177 (2024). 10.1007/s10800-024-02100-4

16 Carrington, M. E. *et al.* Associative pyridinium electrolytes for air-tolerant redox flow batteries. *Nature* **623**, 949–955 (2023). 10.1038/s41586-023-06664-7

17 Marcus, Y. Effect of Ions on the Structure of Water: Structure Making and Breaking. *Chem. Rev.* **109**, 1346–1370 (2009). 10.1021/cr8003828

18 Suo, L. *et al.* "Water-in-salt" electrolyte enables high-voltage aqueous lithium-ion chemistries. *Science* **350**, 938–943 (2015). doi:10.1126/science.aab1595

19 Yamada, Y., Wang, J., Ko, S., Watanabe, E. & Yamada, A. Advances and issues in developing salt-concentrated battery electrolytes. *Nature Energy* **4**, 269–280 (2019). 10.1038/s41560-019-0336-z

20 Sharma, K., Sankarasubramanian, S., Parrondo, J. & Ramani, V. Electrochemical implications of modulating the solvation shell around redox active organic species in aqueous organic redox flow batteries. *Proc. Natl. Acad. Sci. USA* **118** (2021). 10.1073/pnas.2105889118

21 Lim, H.-S. *et al.* Modulating Solvation Structure in Concentrated Aqueous Organic Redox Flow Battery Electrolyte for Solubility and Transport Enhancement via Polycomplex Ion. *ACS Energy Letters* **10**, 2631–2640 (2025). 10.1021/acsenergylett.5c00468

22 Kwabi, D. G., Ji, Y. & Aziz, M. J. Electrolyte Lifetime in Aqueous Organic Redox Flow Batteries: A Critical Review. *Chem. Rev.* **120**, 6467–6489 (2020). 10.1021/acs.chemrev.9b00599

Supplementary Files

This is a list of supplementary files associated with this preprint. Click to download.

- Supplementary.pdf